PHYSICAL REVIEW B **85**, 085421 (2012)

Directing self-assembly of nanostructures kinetically: Patterning and the Ehrlich-Schwoebel barrier

Chuan-Fu Lin,[1] Ajmi B. H. Hammouda,[2] Hung-Chih Kan,[3] N. C. Bartelt,[4] and R. J. Phaneuf[1,*]
[1]*Department of Materials Science and Engineering, University of Maryland, College Park, Maryland 20742, USA*
[2]*Physics Department, Sciences Faculty of University of Monastir, 5019 Monastir, Tunisia*
[3]*Department of Physics, National Chung-Cheng University, Chia-Yi, Taiwan*
[4]*Sandia National Laboratories, Livermore, California 94550, USA*
(Received 5 October 2011; published 13 February 2012)

We present the results of kinetic Monte Carlo simulations of homoepitaxial growth on a patterned substrate in the presence of an extra barrier to a diffusing adatom crossing of steps from above (Ehrlich-Schwoebel barrier) on topographically patterned surfaces. Our results indicate that over a wide range of Ehrlich-Schwoebel barrier heights, incident atom fluxes, and temperatures that multilayer islands or "growth mounds" grow in arrangements which are directed by the topographical pattern. Our simulations indicate that a series of arrangements should form as the temperature is changed due to a competition between the temperature-dependent mound size and the pattern period. We compare these predictions with experimental observation of directed mound assembly on nanopatterned GaAs(001).

DOI: 10.1103/PhysRevB.85.085421 PACS number(s): 81.16.Rf, 81.07.−b, 81.10.−h, 81.15.Jj

A means of fast assembly of extremely large numbers of nanostructures with positional and size control will be required if technology is to keep pace with the ever-decreasing size scale of devices called for by such timetables as Moore's Law[1] and the international technology roadmap for semiconductors.[2] Directed self-assembly,[3] in which a template influences the otherwise spontaneous arrangement of atoms during processes such as growth[4–18] is an appealing candidate for achieving this. Mechanisms by which templates influence control over how atoms assemble are often based upon either local chemistry[3] or strain.[19,20] Here we demonstrate that a qualitatively different type of mechanism, in which an extra diffusion barrier to an atom crossing a step[21,22] can lead to self-assembly of a variety of ordered arrangements of nanometer-sized "mounds" during epitaxial growth on a patterned substrate.

A familiar example of self-assembly is crystal formation, in which atoms align in periodic arrangements which are dictated by local bonding. In this process kinetics limits the degree to which the lowest energy, ordered arrangements can form. On the other hand, kinetic barriers have long allowed for the fabrication of structures in which atoms are not in their lowest free energy configurations. A particularly interesting type of diffusion barrier at step edges[21,22] has been shown to lead both to the formation of multilayer islands or "mounds" during crystal growth[23–30] and step bunching or meandering instabilities during sublimation[31] or growth,[32] respectively. Our recent work on epitaxial growth of GaAs on patterned GaAs(001) substrates showed evidence that this "Ehrlich-Schwoebel" (ES) barrier might play a role in a transient growth instability we observe.[33] Below we investigate the role of the ES barrier during growth on patterned surfaces using kinetic Monte Carlo simulations.

I. METHODS

Our kinetic Monte Carlo simulations are carried out using a Fortran-based code we developed.[34,35] They use a standard solid-on-solid (SOS) description of the growth of a simple cubic crystal. Our SOS model assigns an integer height $z(\vec{R}_{//})$, measured above the average vicinal plane, to each point $\vec{R}_{//}$ on a square grid of dimensions $500a \times 500a$, where a is the lattice constant. We use periodic boundary conditions in both directions. The simulations start with a surface containing a square array of flat-bottomed square pits, each of width 50 lattice constants and with a center-to-center spacing of 100 lattice constants. We start with pits 10 lattice constants deep, bounded by side walls, which form angles of 45° with respect to the surrounding surface.

The microscopic processes considered are the deposition of atoms with an incident flux F and diffusion; desorption is not considered. In most of the results reported here we fixed the incoming flux at a value corresponding to the arrival of 1 monolayer of atoms per second. Absorbed adatoms hop from site to site in the presence of three energetic barriers: the diffusion barrier E_d, the in-plane nearest-neighbor interaction barrier E_a, and the ES barrier E_{ES}, at step edges. The overall barrier to hopping is

$$E_X = E_d + nE_a + \eta E_{\mathrm{ES}}. \tag{1}$$

Here n is the number of nearest-neighbor adatoms with which a diffusing atom interacts; it ranges from 0 to 3, as atoms with 4 neighbors are immobile.[34,35] η is equal to 1 if there is an ES barrier for a particular hop and 0 otherwise. The hopping frequency follows an Arrhenius form with a rate:

$$\Gamma = \nu_0 \exp(-E_X/k_BT), \tag{2}$$

where $\nu_0 = 10^{13}$ Hz is a typical adatom vibration frequency, T is the substrate temperature, and k_{B} is Boltzman's constant. We use typical values for the diffusion barrier and the in-plane nearest-neighbor interaction barrier as 1200 and 300 meV, respectively,[36] and vary E_{ES}. In the simple model used here no preferential diffusion along step edges is considered.

II. RESULTS

Example results of our simulations are shown in Fig. 1. In this case the ES barrier is set equal to 0.1 eV, a typical value for a number of metal surfaces. Figure 1(a) shows the starting surface, while Figs. 1(b)–1(g) show the topography that results after the simulated growth of a film of 1000 monolayers

©2012 American Physical Society

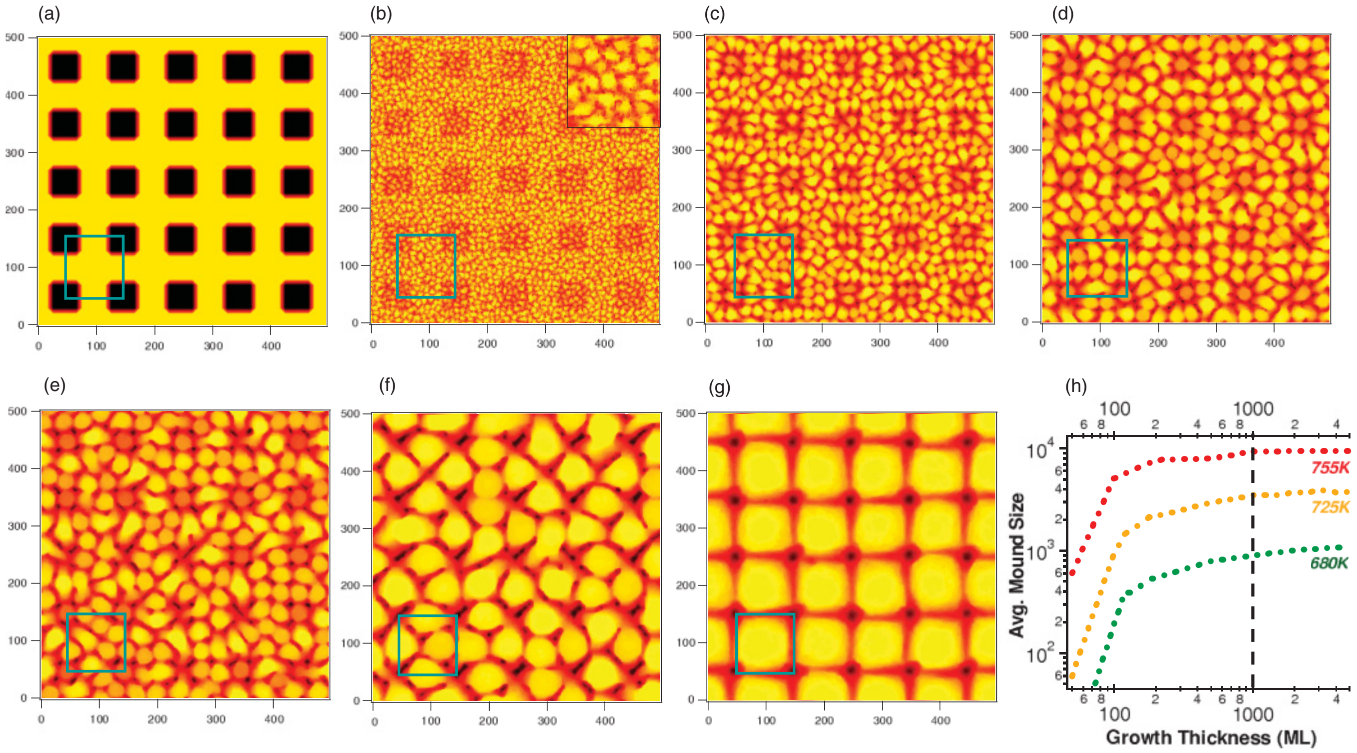

FIG. 1. (Color online) Simulated topography vs growth temperature. (a) Initial patterned surface; pits are 50a wide, 10a deep, and separated by A = 100a center-to-center, where a is the lattice constant. (b)–(g) Simulated topographies after 1000 ML-grown thickness at 1 ML/s. Energetic barriers are Ed = 1.2 eV, Ea = 0.3 eV, EES = 0.1 eV. Growth temperatures are (b) 550 K, (c) 650 K, (d) 680 K, (e) 695 K, (f) 725 K, (g) 755 K, and (h) summary of average mound size vs grown thickness at a series of temperatures; dashed line indicates 1000 ML.

average thickness at rate of 1 ML/s and a series of increasing temperatures. Figure 1(h) summarizes the average mound size vs grown thickness for temperatures across this range and shows that by 1000 monolayers the topography has nearly reached a steady state in each case. Figure 1(b) is for simulated growth at a temperature of 550 K and shows a high density of irregular mounds decorating the surface. The dendritic shapes of individual mounds indicate that diffusive motion of atoms is slow compared to the arrival of new atoms from the flux at this temperature. Increasing the temperature results in the formation of larger mounds of more regular shapes, as can be seen in Figs. 1(c) and 1(d). By 680 K a strong correlation between the positions of the mounds and the original pattern is visibly evident. Further increases in the temperature result in even larger mounds, whose shapes evolve from nearly isotropic, to distinctly diamondlike at 725 K, to square at 755 K. Growing above this temperature produces mounds whose size exceeds that of the pattern cell, and the shapes become less regular.

We statistically analyze the effect of the initial topographical pattern on the self-assembly of the growth mounds, particularly evident in Figs. 1(d), 1(f), and 1(g), using a correlation function, defined as

$$\boldsymbol{G}_2(\vec{\boldsymbol{r}}_{//}) \equiv \langle (z(\vec{\boldsymbol{R}}_{//}) z(\vec{\boldsymbol{R}}_{//} + \vec{\boldsymbol{r}}_{//})) \rangle_{\vec{\boldsymbol{R}}_{//}}. \tag{3}$$

In this expression $z(\vec{R}_{//})$ is the local height of the surface at a particular lateral position $\vec{R}_{//}$, $z(\vec{R}_{//} + \vec{r}_{//})$ is the height at position displaced laterally from this by $\vec{r}_{//}$, and $\langle\rangle_{\vec{R}_{//}}$ denotes the average over all values of $\vec{R}_{//}$. Maps of this correlation function from kinetic Monte Carlo (kMC) simulations of growth at 550, 680, 725, and 755 K are shown in Figs. 2(a)–2(d). The height of the central peak in each of these maps is equal to the mean-square corrugation amplitude, with contributions from both the mounds that assemble spontaneously during growth and what remains of the original pattern. The height of the "first-order" peaks, i.e., those displaced from the map center by a distance equal to the pattern period A along the horizontal ⟨100⟩ and vertical ⟨010⟩ directions, gives a measure of the persistence of the pattern during growth. The most interesting features of these maps are the intermediate, "satellite" peaks whose positions correspond to separations between mounds. The observed series of regular arrays of satellite peaks in the correlation maps confirms the impression obtained from a visual inspection of the simulated images of Fig. 1: arrangement of mounds locks into a series of ordered arrays whose period is related to that of the pattern as the temperature is increased. This behavior is in sharp contrast to what we find for simulated growth on an unpatterned surface. As seen in Figs. 2(e)–2(h) the corresponding correlation maps for such simulations show a nearly isotropic ring surrounding an excluded area around the central peak, but otherwise no indication of ordering of the mounds: the arrangement is "liquidlike." The radius of the ring (R_u) in the correlation maps corresponds to the "natural" nearest-neighbor mound separation.

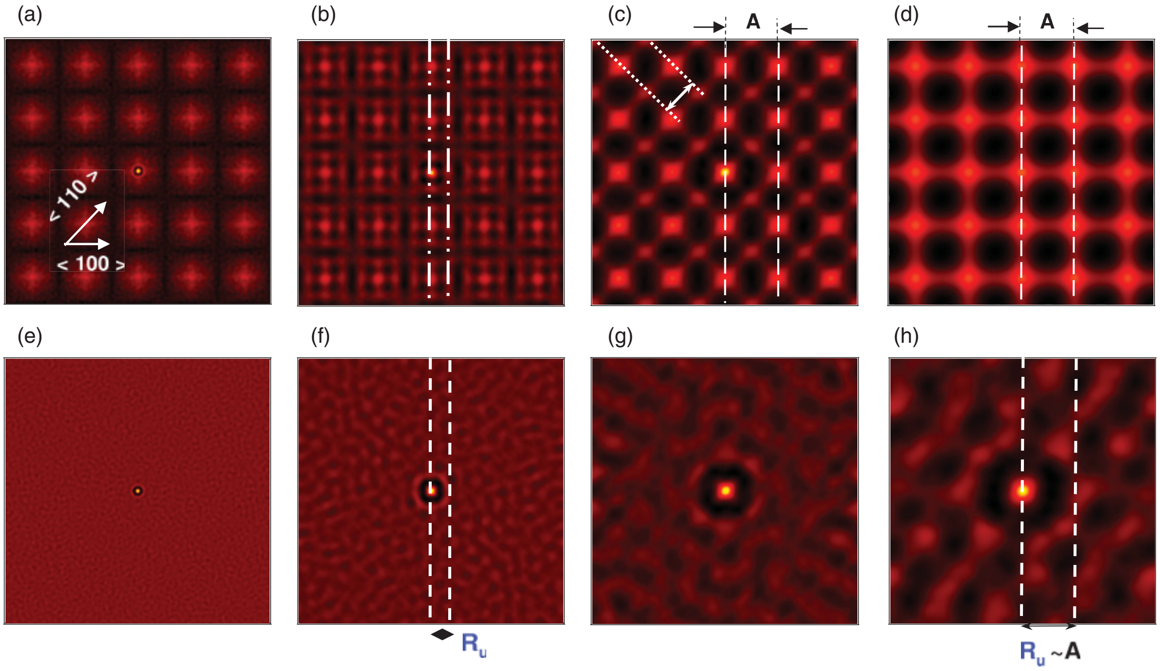

FIG. 2. (Color online) Correlation maps for growth on patterned and unpatterned surfaces after 1000 ML-grown thickness, at 1 ML/s. (a) Growth at 550 K on patterned surface showing weak ordering. (b) Growth on patterned surface at 680 K, showing square ordering; double-dot dash lines show a separation of A/3. (c) Growth on patterned surface at 725 K, showing diagonally ordered structure; dotted lines show a spacing of $\sqrt{2}A/2$. (d) Growth at 755 K on patterned surface showing original pattern period. (e)–(h) Growth on unpatterned initial surface showing liquidlike ordering: (e) at 550 K, (f) at 680 K, (g) at 725 K, (h) at 755 K; R_u indicates the radius of the ring in the correlation maps corresponding to the near-neighbor mound separation.

An analysis of the positions of the satellites as a function of temperature reveals an intriguing behavior in the assembly of mounds when an initial topographical pattern is present. This can be seen in Fig. 3, where we plot the position of the nearest satellite peaks along both the horizontal $\langle 100\rangle$ and diagonal $\langle 110\rangle$ directions vs the radius of the ring on the unpatterned surface. The overall behavior seen here is reminiscent of "devil's staircases," or sequences of higher-order commensurate phases, which form as temperature or pressure are changed in adsorbate systems when there is a competition between preferred adsorbate-spacings and substrate periodicities.[38] For growth at or below 600 K the distances from center of the closest satellites along both of these directions are equal and given by the radius of the ring (R_{u}). At these low temperatures the mound separations are thus isotropic and relatively insensitive to the presence of the pattern, which shows up as a background in the correlation maps. By a growth temperature of 660 K the pattern clearly exerts an influence on the mound spacing: the symmetry of the satellites visually indicates that the mounds assemble into a square lattice, with the ratio of the distances to the nearest diagonal satellite and to the nearest horizontal satellite in the ratio of $\sqrt{2}:1$. Interestingly, the mound lattice has adopted a lattice spacing of A/3, rather than the "natural" value of 0.26A, which it would have in the absence of the pattern. It remains locked into this structure up until a temperature of 700 K, in spite of an increase in the unpatterned mound spacing to 0.43A. An analysis of Figs. 1(d) and 1(e) indicates that there is a strong tendency for a single mound to form within each pit, pinning the arrangement of mounds to that of the pattern, with

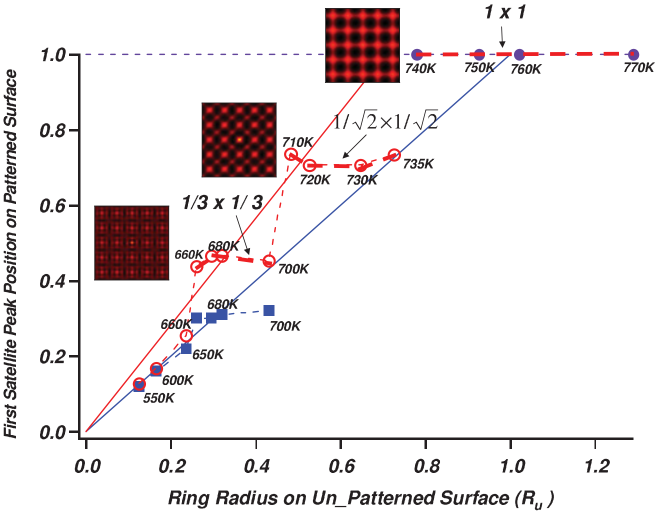

FIG. 3. (Color online) Evidence for lock-in of mounds to series of ordered structures. Nearest satellite peak position from correlation maps after growth on patterned surface vs ring radius for unpatterned surface, along [110] (red open circles) and [100] (blue solid squares). After 1000 ML-grown thickness at 1 ML/s, with temperature as indicated. Solid blue line has slope 1, corresponding to mound spacing along [100] equal to that on an unpatterned surface. Solid red line has slope $\sqrt{2}$. Mound lattice vectors relative to pattern are indicated for three ordered structures. Insets from top to bottom show the correlation maps of surface morphologies after growth at 755, 725, and 680 K, respectively.

two mounds forming in the bridge between pits. Increasing the growth temperature slightly to 710 K causes an abrupt change in the arrangement in which the mounds assemble. Evidently driven by the significantly larger natural spacing, the mound lattice rotates by 45° and adopts an $(A/\sqrt{2} \times A/\sqrt{2})$ unit cell; satellites appear only along ⟨110⟩ directions. The simulated images in this range [e.g., Fig. 1(f)] show that a single mound forms in each bridge-site between near-neighbor pits; mounds do not form within pits at these temperatures. As for the lower temperature $(A/3 \times A/3)$ structure, the mounds lock into this lower coverage structure over a range of temperature, up to 735 K. Raising the temperature to 740 K causes the mounds to assemble into a third, even lower coverage arrangement in which all satellites are absent in the correlation maps. The simulations show that the larger natural spacing of the mounds is accommodated by the assembly of individual mounds in the fourfold sites between pits. At the approximate center of the temperature range for this structure, 755 K, the pattern period A coincides with the spacing mounds would naturally adopt. Increasing the growth temperature above 770 K results in a disordered structure; there is no simple relation of the placement of these large mounds to the topographical pattern, and even the first-order peaks are absent in the correlation maps.

One might wonder how general the series of self-assembled mound structures seen in Figs. 1–3 is. In particular, would a different set of barriers produce mound structures with different periods? To address this we also carried out additional simulations, varying the diffusion barrier (E_d) from 0.8 to 1.2 eV, the in-plane nearest-neighbor interaction barrier (E_a) from 0.25 to 0.4 eV, and the ES barrier (E_{ES}) from 0.05 eV to 0.2 eV. In each case the same sequence of structures occur, although at different temperatures ranges. Evidently these directed self-assembly structures should occur over a range of energy barriers on surfaces and incident fluxes.

Our simulations indicate that it should be possible to use patterning to direct the assembly of nanometer-size mounds into a series of structures in which the spacings are directed by the pattern. What does this mean about the sizes of the mounds? Interestingly, as shown in Fig. 4, we find that the mound sizes show some differences from what might be guessed from the temperature dependence of the correlation map satellite positions. No obvious break in the dependence of the mound size on temperature is seen in the range in which the $(1/3{\times}1/3)$ structure forms. Our analysis shows a continuous decrease in the intensity of the nearest satellite along ⟨100⟩ relative to that along ⟨110⟩ as the temperature is increased from 670 to 700 K, indicating that the mound lattice accommodates the increase in natural size by a continuous increase in the fraction of near-neighbor mound pairs, which are separated along ⟨110⟩ rather than ⟨100⟩ directions in this range. Indeed such a change in the near-neighbor arrangement of mounds is evident by comparing Figs. 1(d) and 1(e).

An interesting question concerns how the choice of initial geometrical parameters might affect which ordered mound arrangements occur for growth on a patterned surface. To investigate this we carried out additional simulations for geometries in which the relative values of different pattern length scales are changed. We find that changing the depth of the pattern at fixed width and pitch has a subtle effect, as summarized in Fig. 5(a) for the case of the same pattern pitch and pit-width as in Figs. 1–3, but with the depth tripled to $h = 30a$. The same sequence of phases as in the $h = 10a$ case occurs, with only changes in the transition regions between them. This may be in part due to the finite sidewall angle which causes a decrease in the widths of the flat mesa widths between pits with increasing pit depth. On the other hand, changing the starting pit-widths for a fixed pitch and depth gives rise to a different sequence of mound structures with increasing temperature. Figure 5(b) summarizes the results for growth simulations in which the pitch and depth are maintained at the same values as in Figs. 1–3, but in which the initial width of the pits is 0.75 times the pitch, i.e., $w = 75a$. In this case the simulations predict four, rather than three ordered mound structures, with unit meshes given by $A/5 \times A/5$, $A/3 \times A/3$, $A/2 \times A/2$, and $A \times A$ as the growth temperature is increased. Interestingly, the rotated $A/\sqrt{2} \times A/\sqrt{2}$ structure is “missing” in this case.

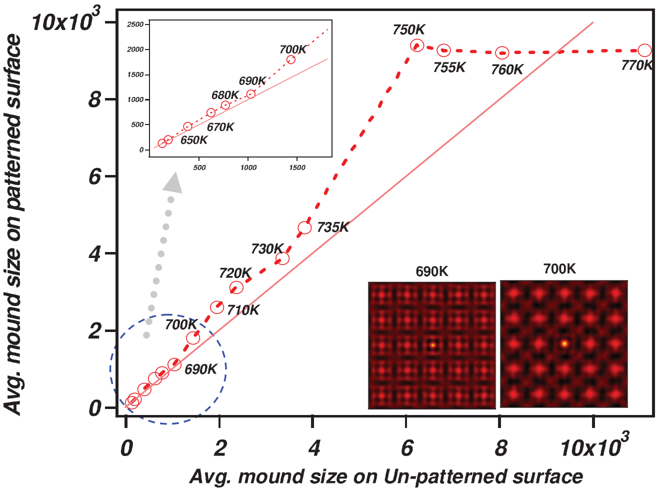

FIG. 4. (Color online) Average mound size on patterned vs unpatterned surfaces. After growth of 1000 ML at 1 ML/s, with temperatures as indicated. Insets at lower right are correlation maps for 690 and 700 K, as indicated.

We do not have a detailed understanding of the relationship between the pattern parameters and the mound structures which form, however, we expect that it involves a competition between a temperature-dependent natural nearest-neighbor mound spacing, discussed previously, and the pattern lateral length scales. The mound-pattern interaction is seemingly based upon the formation of mounds only on the flat mesas around and at the bottoms of pits; this restricts the configurational entropy of mounds on the surface and results in an effective interaction which is entropic in nature.

Are there any real physical systems which show evidence for pattern-directed assembly of growth mounds? The answer is possibly yes. In recent work our group has explored the effect of lithographically patterning GaAs(001) surfaces on the subsequent topography, which evolves as more GaAs is deposited, “homoepitaxial growth.” In our first experiments we used photolithography followed by etching to create patterns

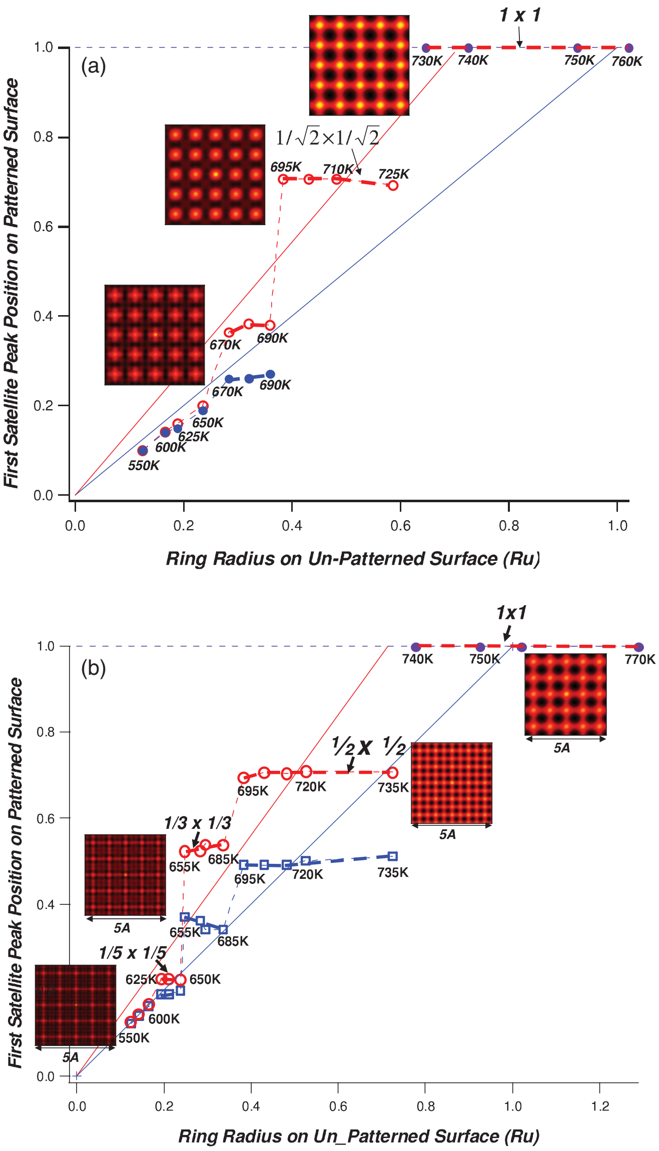

FIG. 5. (Color online) Effect of pattern parameters on sequence of mound structures with temperatures as indicated. Nearest satellite peak position from correlation maps after simulated growth on patterned surface vs ring radius for unpatterned surface, along [110] (red open circles) and [100] (blue solid squares). After 1000 ML-grown thickness at 1 ML/s, with temperature as indicated. (a) Satellite positions for initial pattern pitch $A = 100a$ and width $w = 50a$, as for Fig. 3, but depth increased to $h = 30a$. Insets from top to bottom show the correlation maps of surface morphologies after growth at 740, 710, and 680 K, respectively. (b) Satellite positions for initial pattern pitch $A = 100a$, depth $h = 10a$, and pit width $w = 75a$. Insets from top to bottom show the correlation maps of surface morphologies after growth at 760, 720, 675, and 630 K, respectively.

in which the dimensions and spacings of the pits were microns, much larger than the nanometer scale structures we explored in our simulations. Nevertheless, these experiments produced interesting results which suggest that a small ES barrier is present on these surfaces, at least for steps of a certain orientation. Specifically, on these “micro-patterned” surfaces we found that depositing Ga and As_2 (the latter in excess) at a temperature of 500 °C and a rate of 1 monolayer per second results in the formation of mounds selectively at the edges of pits along [110] directions.[33] At these length scales, the pits are apparently too far apart to result in formation of ordered mound arrangements between them. More recently we have implemented electron beam lithography to make structures whose dimensions and spacings are much smaller, approaching those used in the simulations.

Figure 6 shows a series of atomic force microscopy maps of the topography which results from GaAs growth on such nanopatterned (001) surfaces at two different temperatures. At the lower of the two temperatures, 460 °C, individual mounds span bridges between neighboring pairs of nanopits separated along [110] directions, (“[110] twofold bridges”). It is at these same sites that mounds form in the second ordered arrangement, $A/\sqrt{2} \times A/\sqrt{2}$ structure, in the simulations for the first pattern geometry discussed previously [Fig. 1(f)]. A difference is that the mounds which form at the centers of the twofold bridges along $[1\bar{1}0]$ directions in the simulations are missing in the experiments. The GaAs(001) surface in fact is not fourfold symmetric: both the Ga diffusivity[37,39] and adatom-step sticking probabilities[40] are different along [110] and $[1\bar{1}0]$, as is the geometry of steps running along [110] (“B-type”) and $[1\bar{1}0]$ (“A-type”) for both the $c(4\times4)$[37] of interest here and the $\beta2(2\times4)$ reconstruction,[39–44] which occurs above ∼550 °C.[33,45] In addition, our earlier results on micropatterned GaAs(001) suggested the presence of a finite ES barrier along [110] but not obviously along $[1\bar{1}0]$. The height variations visible as gray belts in Fig. 6(b) and 6(c) reflect these effects; even more striking is the observation after increasing the experimental growth temperature to 525 °C. In this case mounds again form at the centers of the fourfold bridges between the corners of nanopit neighbors and lead to the same $A \times A$ structure seen at the higher temperatures in the simulations [Fig. 1(g)]. Additional preliminary experiments at lower temperatures than those explored here suggest that directed assembly of higher density mound structures is possible as well.[45]

III. DISCUSSION

We now consider how an artificially imposed topographical pattern might act in directing the assembly of mounds during growth. One possibility is based upon the modification of the local density of adatoms on the surface. On relatively flat regions of a surface such as those between the pits, growth via the formation of atom clusters (“islands”) is favored over the addition of atoms to existing steps. As islands are most likely to form where adatom density is high, a seeming explanation for our observations is that the positions of the maxima in the adatom density relative to the pattern changes with temperature owing to thermal activation across the ES barriers at the edges of pits. This possibility, however, is ruled out by a simple solution of the diffusion equation, which shows that initially the adatom density is always at the fourfold bridge sites; a moderate ES barrier flattens this maximum out but does not shift its position.[46] Initially this favors island formation near the centers of the bridges between pits. We thus consider a second possibility, suggested by the inset of

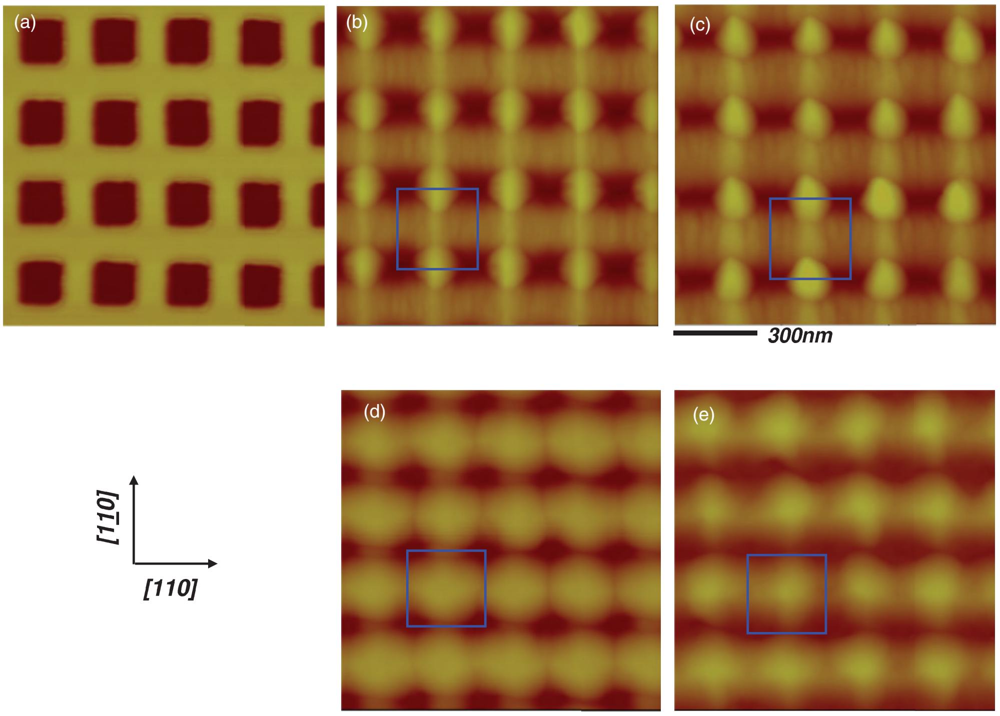

FIG. 6. (Color online) Mound structures during growth of GaAs on nanopatterned surfaces. (a) Atomic force microscope image of topography of patterned GaAs(001) before growth. Pits are 30 nm deep, 150 nm wide, and spaced at A = 300 nm. (b) AFM image after growth of 60 nm of additional GaAs at 460 °C. The blue square shows the unit cell of the initial square pattern. (c) After growth of 100 nm at 460 °C. (d) After growth of 30 nm, at a temperature of 525 °C. (e) After growth of 60 nm at 525 °C.

Fig. 4, that beneath 700 K the mound sizes on the patterned surfaces follow those determined by kinetics in the absence of a pattern. This natural size arises from the competition of the ES barrier, which favors vertical growth of multi-island stacks[24–31] and arrival of diffusing adatoms on the underlying surface favors lateral growth due to attachment to the edges of the bottom-most island. For this to be the correct explanation the mound positions would need to evolve during growth from the initial nucleation sites favored by highest adatom density to relative positions determined by their natural size and the effects of the pattern. One of these is the reduction of the area of the underlying terrace, and thus the supply of adatoms for lateral growth, if a mound approaches the upper edge of a pit. Some evidence for this evolution is seen in Fig. 7, which shows series of height profiles from our simulations for increasing grown thickness. Successive panels in this figure are for temperatures corresponding to the centers of the ranges in which the three ordered mound structures

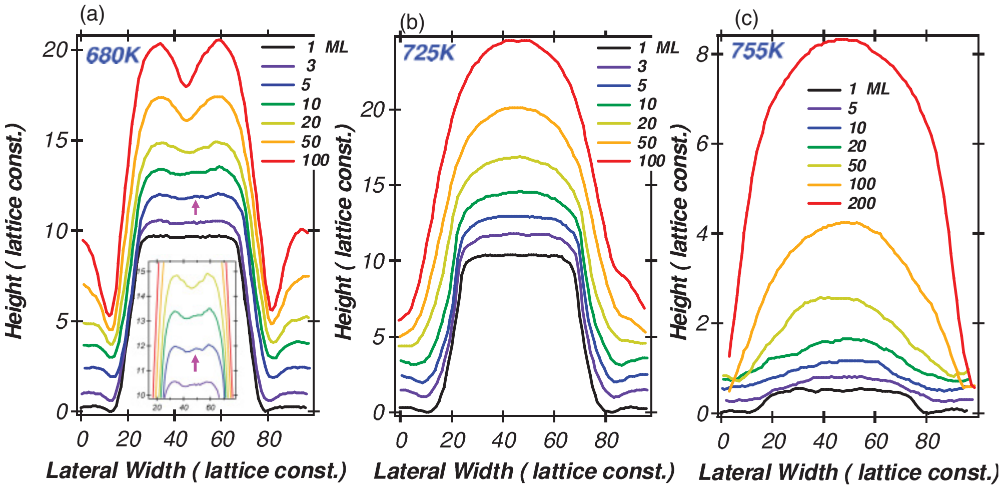

FIG. 7. (Color online) Height profiles of simulated surfaces for increasing amounts of growth. (a), (b) Evolution of morphologies of the twofold bridges at growth temperatures 680 and 725 K; the arrow in (a) indicates a local height maximum near the center of twofold bridges at initial stage of growth. (c) Evolution of morphologies of the fourfold bridges. The heights of profiles are rescaled to display subtle features at the early growth stage.

assemble for the pattern geometry of Fig. 1. For the $A/3 \times A/3$ arrangement of mounds seen in Fig. 1(d), two mounds can be accommodated in the bridge between near-neighbor pits, with a third forming in the pit bottoms; in Fig. 7(a) an initial height maximum forms near the center of the twofold bridge, as expected based on the adatom density, but two maxima evolve near the bridge edges as the growth continues. Raising the temperature increases the rate of atom diffusion, and thus the natural size of the mounds. Larger mounds are accommodated by the twofold bridge sites in the $A/\sqrt{2} \times A/\sqrt{2}$ structure, and the largest in the fourfold bridge sites of the $A\times A$ structure.

The model used in our simulations is extremely simple and leaves out many effects, including elastic strain near the edges of pits, interaction between steps like those that bound the pits and anisotropy in the diffusivity, and atom-step attachment probabilities. Nonetheless the simulations, along with early experimental results, suggest that indeed the extra ES barrier, which impedes atoms crossing steps from above and has been long known to produce mounds during growth on certain surfaces,[24–31] might be exploited to direct the arrangement of such mounds on a patterned surface.

IV. CONCLUSIONS

In summary, our results show that a purely kinetic effect, i.e., an additional diffusion barrier at step edges, can act not merely to suppress the lowest energy atom arrangement during growth but to direct a series of ordered arrangements of nanometer-sized mounds with temperature by controlling the competition between the natural mound near neighbor spacing and the length scales imposed by an artificially produced pattern. The sequence of mound structures varies with the pattern length scales. Most importantly, the density of mounds in these structures can exceed that of the initial pattern. We anticipate that this phenomenon could find application in the fast, controlled assemblies of nanostructures called for by current technology.

ACKNOWLEDGMENTS

This work was supported by the National Science Foundation (No. DMR-0705447), the Laboratory for Physical Sciences, and the NSF-MRSEC at the University of Maryland (No. DMR-0520471). We acknowledge helpful conversations with S. V. Khare and S. Kanakaraju and C. J. K. Richardson for help with the growth experiments.

---

[*] phaneuf@umd.edu

[1] G. E. Moore, Electronics **38**, 114 (1965).

[2] H. S. Bennett, J. Res. National Institutes of Standards and Technology **112**, 25 (2007).

[3] See, for example, S. Mann, Nat. Mater. **8**, 781 (2009).

[4] T. I. Kamins and R. S. Williams, Appl. Phys. Lett. **71**, 1201 (1997).

[5] A. Konkar, R. Heitz, T. R. Ramachandran, P. Chen, and A. Madhukar, J. Vac. Sci. Technol. B **16**, 1334 (1998).

[6] R. Zhang, R. Tsui, K. Shiralagi, D. Convey, and H. Goronkin, Appl. Phys. Lett. **73**, 505 (1998).

[7] G. Jin, J. L. Liu, and K. L. Wang, Appl. Phys. Lett. **76**, 3591 (2000).

[8] H. Lee, J. A. Johnson, M. Y. He, J. S. Speck, and P. M. Petroff, Appl. Phys. Lett. **78**, 105 (2001).

[9] T. Kitajima, B. Liu, and S. R. Leone, Appl. Phys. Lett. **80**, 497 (2002).

[10] T. Ogino, Y. Homma, Y. Kobayashi, H. Hibino, K. Prabhakaran, K. Sumitomo, H. Omi, S. Suzuki, T. Yamashtia, D. J. Bottomley, F. Ling, and A. Kaneko, Surf. Sci. **514**, 1 (2002).

[11] Z. Y. Zhong, A. Halilovic, M. Mühlberger, F. Schäffler, and G. Bauer, Appl. Phys. Lett. **82**, 445 (2003).

[12] Z. Y. Zhong, A. Halilovic, M. Mühlberger, F. Schäffler, and G. Bauer, J. Appl. Phys. **93**, 6258 (2003).

[13] Z. Y. Zhong, A. Halilovic, T. Fromherz, F. Schäffler, and G. Bauer, Appl. Phys. Lett. **82**, 4779 (2003).

[14] J. L. Gray, S. Atha, R. Hull, and J. A. Floro, Nano Lett. **4**, 2447 (2004).

[15] B. Yang, F. Liu, and M. G. Lagally, Phys. Rev. Lett. **92**, 025502 (2004).

[16] R. V. Kukta, G. Petroff, and D. Kouris, J. Appl. Phys. **97**, 033527 (2005).

[17] J. L. Gray, R. Hull, and J. A. Floro, J. Appl. Phys. **100**, 084312 (2006).

[18] A. Pascale, I. Berbezier, A. Ronda, and P. C. Kelires, Phys. Rev. B **77**, 075311 (2008).

[19] A. T. N'Diaye, S. Bleikamp, P. J. Feibelman, and T. Michely, Phys. Rev. Lett. **97**, 215501 (2006).

[20] H. Hu, H. J. Gao, and F. Liu, Phys. Rev. Lett. **101**, 216102 (2008).

[21] G. Ehrlich and F. G. Hudda, J. Chem. Phys. **44**, 1039 (1966).

[22] R. L. Schwoebel and E. J. Shipsey, J. Appl. Phys. **37**, 3682 (1966).

[23] M. D. Johnson, C. Orme, A. W. Hunt, D. Graff, J. L. Sudijono, L. M. Sander, and B. G. Orr, Phys. Rev. Lett. **72** 116 (1994).

[24] P. Politi and J. Villain, Phys. Rev. B **54**, 5114 (1996).

[25] J. Camarero, V. Cross, M. J. Capitán, J. Álvarez, S. Ferrer, M. A. Niño, J. E. Prieto, L. Gómez, J. Ferrón, A. L. Vázquez de Parga, J. M. Gallego, J. J. de Miguel, and R. Miranda, Appl. Phys. A **69**, 553 (1999).

[26] S. Schinzer, S. Kohler, and G. Reents, Eur. Phys. J. B **15**, 161 (2000).

[27] M. Vladimirova, A. Pimpinelli, and A. Videcoq, J. Cryst. Growth **222**, 631 (2000).

[28] H. C. Kan, S. Shah, T. T. Tadyyon-Eslami, and R. J. Phaneuf, Phys. Rev. Lett. **92**, 146101 (2004).

[29] Z.-J. Liu and Y. G. Shen, Surf. Sci. **595**, 20 (2005).

[30] A. B. H. Hamouda, A. Pimpinelli, and R. J. Phaneuf, Surf. Sci. **602**, 2819 (2008).

[31] J. Krug, V. Tonchev, S. Stoyanov, and A. Pimpinelli, Phys. Rev. B **71**, 045412 (2005).

[32] G. S. Bales and A. Zangwill, Phys. Rev. B **41**, 5500 (1990).

[33] T. Tadayyon-Eslami, H. C. Kan, L. C. Calhoun, and R. J. Phaneuf, Phys. Rev. Lett. **97**, 126101 (2006).

[34] A. Ben-Hamouda, N. Absi, P. E. Hoggan, and A. Pimpinelli, Phys. Rev. B **77**, 24530 (2008).

[35] A. B. Hamouda, A. Pimpinelli, and T. L. Einstein, Surf. Sci. **602**, 3569 (2008).

[36] These values are close to those based upon first principles calculations for $c(4 \times 4)$-GaAs(001) by Roehl *et al.*, Ref. 37.

[37] J. L. Roehl, A. Kolagatla, V. K. K. Ganguri, S. V. Khare, and R. J. Phaneuf, Phys. Rev. B **82**, 165335 (2010).

[38] P. Bak, Rep. Prog. Phys. **45**, 587 (1982).

[39] M. Itoh, Phys. Rev. B **64**, 045301 (2001).

[40] T. Shitara, D. D. Vvedensky, M. R. Wilby, J. Zhang, J. H. Neave, and B. A. Joyce, Phys. Rev. B **46**, 6825 (1992).

[41] G. R. Bell, T. S. Jones, and B. A. Joyce, Surf. Sci. **429**, L492 (1999).

[42] M. Itoh and T. Ohno, Phys. Rev. B **63**, 125301 (2001).

[43] M. Itoh, G. R. Bell, A. R. Avery, T. S. Jones, B. A. Joyce, and D. D. Vvedensky, Phys. Rev. Lett. **81**, 633 (1998).

[44] T. Shitara, J. Zhang, J. H. Neave, and B. A. Joyce, J. Appl. Phys. **71**, 4299 (1992).

[45] C. F. Lin, H. C. Kan, S. Kanakaraju, C. J. K. Richardson, N. C. Bartelt, and R. J. Phaneuf (unpublished).

[46] N. C. Bartelt (unpublished).